1521-0103/349/3/393–401$25.00
THE JOURNAL OF PHARMACOLOGY AND EXPERIMENTAL THERAPEUTICS

http://dx.doi.org/10.1124/jpet.114.214098
J Pharmacol Exp Ther 349:393–401, June 2014

Bryostatin-1 Restores Hippocampal Synapses and Spatial Learning and Memory in Adult Fragile X Mice

Miao-Kun Sun, Jarin Hongpaisan, Chol Seung Lim, and Daniel L. Alkon

Blanchette Rockefeller Neurosciences Institute, Morgantown, West Virginia

Received February 21, 2014; accepted March 20, 2014

ABSTRACT

Fragile X syndrome (FXS) is caused by transcriptional silencing in neurons of the *FMR1* gene product, fragile X mental retardation protein (FMRP), a repressor of dendritic mRNA translation. The lack of FMRP leads to dysregulation of synaptically driven protein synthesis and impairments of intellect, cognition, and behavior, a disorder that currently has no effective therapeutics. Fragile X mice were treated with chronic bryostatin-1, a relatively selective protein kinase ε activator with pharmacological profiles of rapid mGluR desensitization, synaptogenesis, and synaptic maturation/repairing. Differences in the major FXS phenotypes, synapses, and cognitive functions were evaluated and compared among the age-matched groups. Long-term treatment with bryostatin-1 rescues adult fragile X mice from the disorder phenotypes, including normalization of most FXS abnormalities in hippocampal brain–derived neurotrophic factor expression and secretion, postsynaptic density–95 levels, glycogen synthase kinase–3β phosphorylation, transformation of immature dendritic spines to mature synapses, densities of the presynaptic and postsynaptic membranes, and spatial learning and memory. Our results show that synaptic and cognitive function of adult FXS mice can be normalized through pharmacologic treatment and that bryostatin-1-like agents may represent a novel class of drugs to treat fragile X mental retardation even after postpartum brain development has largely completed.

Introduction

Fragile X syndrome (FXS) is the most common monogenically inherited form of intellectual disability (Kaufmann et al., 1999; Santoro et al., 2012). The FXS includes general deficits in cognition (Van der Molen et al., 2010; Yang et al., 2013), abnormal in memory (Koekkoek et al., 2005), and anxiety and autistic-like behavior (Sabaratnam et al., 2003; Garber et al., 2008).

In nearly all of the cases, FXS is caused by an expansion of an untranslated CGG repeat in the 5′-untranslated region of the X-linked gene fragile mental retardation 1 (*FMR1*; Verkerk et al., 1991; Ludwig et al., 2014). The expansion leads to DNA methylation of *FMR1* and transcriptional silencing, thus loss of the fragile X mental retardation protein (FMRP). FMRP is a selective RNA-binding protein (Schaeffer et al., 2003), regulating the translation of dendritic mRNAs (Ashley et al., 1993; Darnell and Klann, 2013; Gonçalves et al., 2013).

The lack of FMRP alters signal processing at synapses, such as that involving metabotropic glutamate receptor (mGluR) signaling (Weiler et al., 1997; Lüscher and Huber, 2010; Bhattacharya and Klann, 2012). The leading "mGluR theory of FXS" proposes that overactive mGluR signaling, normally balanced by FMRP, underlies much of the brain changes of FXS (Bhogal and Jongens, 2010; McLennan et al., 2011; Santoro et al., 2012; Hajós, 2014). Indeed, a mouse model that combines *FMR1* inactivation with a 50% reduction in *mGluR5* expression rescues several anatomic and behavioral consequences of FXS. mGluR5 antagonism has also been shown effective in several FXS phenotypes (Connor et al., 2011; Vinueza Veloz et al., 2012; Hajós, 2014).

One of the major goals of FXS research is to develop effective therapies. Despite extensive efforts, therapeutic options for FXS remain limited. Although preclinical studies with mGluR5 antagonism appear promising, therapeutic values of mGluR inhibitors for FXS are still not clear. One problem with inhibition of the mGluR signaling, for instance, is that the inhibition exaggerates spine immaturity in the fragile X mice (Cruz-Martin et al., 2010), an effect opposite to the intended therapeutic outcomes. Here, we show that bryostatin-1 (Nelson et al., 2009; DeChristopher et al., 2012), a highly potent and relatively specific protein kinase C (PKC) ε activator (also of PKCα), with pharmacologic profiles of rapid mGluR desensitization, synaptogenesis, and synaptic maturation/repairing (Hongpaisan and Alkon, 2007; Sun et al., 2008; Hongpaisan et al., 2011), rescues synaptic and memory functions and other phenotypic features in adult fragile X mice. Bryostatin-1 has a much lower ED_{50} for inducing PKCε translocation than its ED_{50}s for PKCα or PKCδ (Szallasi et al., 1994). The structural features of the bryostatins have been well defined by leading experts in

The authors claim no conflict of interest.
dx.doi.org/10.1124/jpet.114.214098.

ABBREVIATIONS: BDNF, brain-derived neurotrophic factor; DiI, 1,1′-dioctadecyl-3,3,3′,3′-tetramethylindocarbocyanine perchlorate; ELISA, enzyme-linked immunosorbent assay; *FMR1*, fragile mental retardation gene 1; FMRP, fragile X mental retardation protein; FXS, fragile X syndrome; GAP, growth-associated protein; GSK, glycogen synthase kinase; mGluR, metabotropic glutamate receptor; PBS, phosphate-buffered saline; PKC, protein kinase C; PSD, postsynaptic density; TBS-T, Tris-buffered saline plus 0.1% Tween 20.

function-oriented synthesis (Wender et al., 1988, 2011). Bryostatin-1–like agents may represent a novel class of drugs for treating FXS.

Materials and Methods

Animals and Drug Treatment. Two types of mice (male; The Jackson Laboratory, Bar Harbor, ME; 9 or 10/group) were used as follows: FVB.129P2-*Pde6b*$^{+}$ *Tyr*$^{c\text{-}ch}$ *Fmr1*^{tm1Cgr}/J (formerly identified as FVB.129P2-*Fmr1*^{tm1Cgr}/*J* or fragile X mice) and FVB.129P2-*Pde6b*$^{+}$ *Tyr*$^{c\text{-}ch}$/AntJ (as the controls). These mice do not suffer from blindness. They were housed in a temperature-controlled (20–24°C) room for at least a week, allowed free access to food and water, and kept on a 12-hour light/dark cycle.

All mice were randomly assigned to different groups. We began to treat the fragile X mice when they reached an age of 2 months with bryostatin-1 (20 μg/m^2, tail i.v., two doses/week for 13 weeks). The dose was chosen, based on our preliminary dose-response studies showing that smaller doses were not effective against induced synaptic and cognitive impairments. Nontreated groups received the same volume of vehicle at the same frequency. Synaptic and memory functions and other phenotypic features were evaluated 10 days after the last dose.

Total RNA Isolation and Reverse Transcription–Polymerase Chain Reaction. Bilateral hippocampi were dissected ($n = 5$) for total RNA isolation, using an RNeasy Mini kit (Qiagen, Valencia, CA). RNA purity was confirmed by spectrophotometry ($A_{260}/A_{280} > 1.8$), and RNA integrity was visualized by agarose gel electrophoresis. For reverse transcription–polymerase chain reaction (RT-PCR), 500 ng of total RNA was reverse-transcribed, using oligo(dT) primer and Superscript III (Invitrogen, Carlsbad, CA) at 50°C for 1 hour. Real-time PCR was performed for 40 cycles with SYBR Green I PCR Master mixture and processed on a LightCycler 480 II (Roche, Indianapolis, IN) machine. The following primers (Origene, Rockville, MD) were used: mouse BDNF, 5′-GGCTGACACTTTTGAGCACGTC-3′ and 5′-CTCCAAAGGCACTTGACTGCTG-3′ and mouse GAPDH, 5′-TGAACGGGAAGCTCACTGGCAT-3′ and 5′-TCAGATGCCTGCTTCACCACCT-3′ as a control. Threshold cycle (Ct) for BDNF was normalized on the housekeeping GAPDH (dCt), and every experimental sample was referred to its control (ddCt). Relative change values were expressed as $2^{-\mathrm{ddCt}}$.

Western Blot Analysis. Bilateral hippocampi ($n = 5$) were homogenized in ice-cold lysis buffer—10 mM Tris-Cl, pH 7.4, 5 mM EDTA, 1% SDS, and 1× complete protease inhibitor cocktail (Thermo Fisher Scientific, Waltham, MA). After protein concentration measurement with the BCA method, the same number of proteins (25 μg/lane) was then separated using 18% (for BDNF) or 8% (for FMRP, PSD-95, GSK-3β, phospho-GSK-3β [Ser9], and α-tubulin) SDS-PAGE gel and transferred onto nitrocellulose membranes (Invitrogen). The membranes were blocked in 5% nonfat dry milk in Tris-buffered saline plus 0.1% Tween 20 (TBS-T) for 1 hour and then incubated with rabbit anti-BDNF (1:500; Santa Cruz Biotechnology, Inc., Santa Cruz, CA), rabbit FMRP (1:1000; Cell Signaling Technology, Danvers, MA), mouse anti-PSD-95 (1:1000; Santa Cruz Biotechnology), rabbit GSK-3β (1:1000; Cell Signaling Technology), and rabbit phospho-GSK-3β (Ser9) (1:1000; Cell Signaling Technology) in TBS-T overnight at room temperature. After three washes with TBS-T, the membranes were incubated with horseradish peroxidase–conjugated anti-rabbit or mouse immunoglobulin G (IgG) (1:5000; Jackson ImmunoResearch Laboratories, West Grove, PA) in TBS-T for 1 hour at room temperature, and immunoreactive bands were visualized by SuperSignal West Pico chemiluminescent substrate. To control for loading differences across lanes, membranes were stripped and reprobed using mouse anti–α-tubulin (1:5000; Sigma-Aldrich) and horseradish peroxidase–conjugated anti-mouse IgG (1:5000; Jackson ImmunoResearch Laboratories). Levels of immunoreactivity were assessed by densitometric analysis of films, using the ImageJ 1.44a system, and normalized to α-tubulin levels.

Enzyme-Linked Immunosorbent Assay. Bilateral hippocampi were homogenized in ice-cold homogenization buffer consisting of 20 mM Tris-Cl (pH 7.4) buffer containing 137 mM NaCl, 1% Triton X-100, 10% glycerol, and 1× protease inhibitor cocktail (Thermo Fisher Scientific) and used for measuring BDNF. The homogenates were centrifuged at 14,000*g* for 30 minutes. From the resulting supernatants, total BDNF amounts were measured with the mouse BDNF ELISA technique (Insight Genomics).

Confocal Microscopy for Dendritic Spine Morphology. Mice were deeply anesthetized with chloral hydrate (400 mg/kg i.p.) and perfused through the heart by gravity with phosphate buffered saline (PBS) at room temperature. They were then perfused with 4% paraformaldehyde in PBS (20 ml for light fixation) at room temperature to avoid the negative impact of hypothermia on the number of dendritic spines (Kirov et al., 2004). Right dorsal hippocampi were dissected and sectioned with a vibratome (Leica VT1000S). A series of sections were selected from the right dorsal hippocampi by starting at approximately 1200 μm and selecting one section every 400 μm.

The number of distinct shapes of dendritic spines on individual dendritic shafts was studied with 1,1′-dioctadecyl-3,3,3′,3′-tetramethylindocarbocyanine perchlorate (DiI; Invitrogen) staining, as previously described (Hongpaisan and Alkon, 2007).

Dendritic spines in the stratum radiatum were imaged (>510 nm/568 nm; excitation/emission) with a Zeiss Axio Observer Z1 microscope equipped with a 710 confocal scanning system, using the 100× Plan-APO Chromat oil immersion objective (1.4 numerical aperture). A series of randomized confocal images (1024 × 1024 pixels) were confocally scanned every 0.45 μm. Individual spines identified on a single image were verified on adjacent images of series of confocal images to approximate the three-dimensional structure of the spines with the ImageJ program (http://rsb.info.nih.gov/ij/). The criteria to differentiate the morphology of dendritic spines were based on the relative ratios between spine, head, and neck lengths, as described by Sorra and Harris (2000).

Densities of Pre- and Postsynaptic Structures and BDNF Immunohistochemistry. For immunohistochemical studies, hippocampal sections were incubated free-floating overnight at room temperature with primary antibodies (Millipore/Chemicon, Billerica, MA): mouse monoclonal anti–growth-associated protein (GAP)-43/B-50 (1:2000), polyclonal rabbit anti-neurogranin (1:400), and mouse monoclonal anti-synaptophysin (1:2000). Tissue sections were then incubated with either Alexa Fluor 568 goat anti-rabbit IgG (1:200; Invitrogen) for 3 hours at room temperature or biotinylated anti-mouse secondary antibody (1:20; Vector Laboratories, Burlingame, CA) for 3 hours at room temperature and then streptavidin-conjugated Alexa Fluor 488 (1:100; Invitrogen) for 3 hours at room temperature. Sections were mounted with VECTASHIELD mounting medium (Vector Laboratories) with 4′,6-diamidino-2-phenylindole to counterstain nuclei.

Confocal images (Zeiss confocal microscope, 63× objectives) were acquired of hippocampal sections between 0.6-μm thick, in-line scan mode, and with a pinhole of approximately 1.00 Airy unit. Confocal images with similar levels of 4′,6-diamidino-2-phenylindole fluorescence intensity were quantified with the ImageJ program.

The densities per 63 × 63 × 0.6 μm^3 volume of the CA1 stratum radiatum (where apical dendrites of CA1 pyramidal neurons are located) of postsynaptic membranes (neurogranin grains), presynaptic membranes (GAP-43 grains), presynaptic axonal terminals (the presynaptic vesicle membrane protein synaptophysin grains), and presynaptic vesicle concentration (synaptophysin fluorescence intensity) were measured. The microscope lateral resolution was 20 nm in XY and 100 nm in Z, and its point-spread function was automatically collected by the microscope software. By collecting confocal images at 0.6-μm thickness, the overlap of synaptic membranes or axonal boutons was minimized.

Electron Microscopy. Electron microscopy was used to evaluate synaptic details. Mice at an age of 2 months were treated with bryostatin-1 (25 μg/kg i.p., twice/week) for 5 weeks. Under anesthesia

(pentobarbital, 80 mg/kg i.p.), mice were perfused through the left cardiac ventricle with phosphate-buffered saline by gravity and then fixed with 2.5% glutaraldehyde and 3% paraformaldehyde in PBS at room temperature. Right dorsal hippocampi were dissected and sectioned with a vibratome slicer at 400-μm thickness. The hippocampal sections were resectioned to 100-μm thickness and washed three times with ice-cold PBS and postfixed in ice-cold 1% OsO4 for 1 hour and then rinsed with ice-cold distilled water. Hippocampal slices were dehydrated in an ice-cold, graded ethanol series. Sections were followed by resin embedding at room temperature. Ultrathin sections (70 nm) were stained with uranyl acetate and lead acetate and viewed with a Zeiss Libra 120+ electron microscope. Random sampling to determine synaptic density was achieved by orienting the hippocampal CA1 area under low-power magnification. The random area that immediately appeared after switching to a higher magnification (8000× magnification and a pixel resolution of 266.859 pixels/μm) was imaged with a charge-coupled device camera (UltraScan, Gatan, Pleasanton, CA).

During double-blind quantification, electron micrographs (64 μm^2 CA1 area at 8000×) were digitally zoomed up to 16,000× magnification by the Preview program in a Mac Pro computer with a Mac OS X operating system and a 30-inch monitor. Spines were defined as structures that do not have mitochondria and form synapses with axon boutons that contain presynaptic vesicles.

Spatial Learning and Memory and Visible Platform Test. A modified water maze task (two trials per day for 8 days), a difficult task for revealing mild impairments, was used to evaluate spatial learning and memory.

The training for the water maze task began on the 10th day after the last dose of bryostatin-1, a time gap to separate potential acute effects of the agent from the chronic therapeutic impacts. The maze pool had a diameter of 114 cm and height of 60 cm and was filled with 40 cm H_2O (22 ± 1°C), mixed with 200 ml of nontoxic white Tempera (BesTemp, Certified Color Corp, Orange, CA). Mice were trained to find a hidden platform, centered in one of the quadrants and submerged ~ 2 cm below the water surface. At the start of all trials, mice were placed individually in the water facing the maze wall, using different starting positions each trial, and allowed to swim until they found the platform where they remained for 20 seconds. A mouse that failed to find the platform within 1.5 minutes was guided there by the investigator, with 90 seconds scored. The swim path was recorded with a video-tracking system. After the training trials, a probe trial was given, 24 hours after the last training trial, with the platform removed to assess memory retention for its location by the distance the mouse moved in the quadrants. The video-tracking system tracked the animal's movements in each quadrant during a period of 1 minute.

A visible platform test was used to evaluate the sensorimotor abilities of each mouse. The platform was placed at a new location and was marked with a pole that protruded 9 inches above the water surface. The escape latency and the route of the mouse's swimming across the pool to the visible platform were recorded with the video-tracking system.

Statistical analysis was performed using the analysis of variance, followed by Newman-Keuls multiple comparisons test. $P < 0.05$ was considered statistically significant. All procedures were conducted according to National Institutes of Health *Guide for the Care and Use of Laboratory Animals* and approved by the Ethics Committee of the Institute.

Results

Bryostatin-1 Increases BDNF Levels, PSD-95, and GSK-3β Phosphorylation. FMRP was only highly expressed in the wild type, but not in the fragile X mice (Fig. 1A). Bryostatin-1 had no significant impact on its expression (Fig. 1A).

The quantitative RT-PCR study revealed that the hippocampal *BDNF* mRNA levels did not differ significantly between the fragile X mice and the wild type. Bryostatin-1 increased the *BDNF* mRNA level by approximately 2.1-fold in the wild type ($F_{1,58} = 19.64$, $P < 0.001$) and by approximately 2-fold in the fragile X mice ($F_{1,58} = 17.23$, $P < 0.001$; Fig. 1B).

The BDNF protein levels in hippocampal extracts were measured with Western blot analysis. Bryostatin-1 increased production of the 14-kDa BDNF form by ~45% in the wild type ($F_{1,28} = 4.727$, $P < 0.05$) and 44% ($F_{1,28} = 4.59$, $P < 0.05$) in the fragile X mice, respectively (Fig. 1C). By use of the sandwich ELISA method, no significant differences were found between the untreated groups, but bryostatin-1 enhanced BDNF production by ~2.43-fold ($F_{3,156} = 8.682$, $P < 0.001$; Fig. 1D). By use of immunohistochemistry and confocal microscopy, we also observed significant group differences in BDNF expression (Fig. 1E; $F_{3,114} = 3.633$, $P < 0.01$). Bryostatin-1 restored BDNF levels in the hippocampal CA1 stratum radiatum in the fragile X mice (Fig. 1F).

We determined the expression of PSD-95, a postsynaptic marker protein, to explore whether bryostatin-1 can rescue functional synapses. PSD-95 expression decreased in the hippocampus of the fragile X mice by 34% ($F_{1,28} = 4.289$, $P < 0.05$, versus the wild type; Fig. 1G). Bryostatin-1 enhanced PSD-95 expression by ~51% ($F_{1,28} = 4.935$, $P < 0.05$) and rescued the PSD-95 levels in the fragile X mice ($F_{1,28} = 7.793$, $P < 0.01$; Fig. 1G).

GSK-3β is highly active in FXS and is one of the core phenotypes of FXS. There were no group differences in the total GSK-3β levels. However, levels of phosphorylation of GSK-3β on Ser9 were lower by approximately 33% in the hippocampus of the fragile X mice ($F_{1,28} = 9.884$, $P < 0.01$; Fig. 1H), indicating that GSK-3β was more active in the hippocampus of the fragile X mice. Bryostatin-1 increased phosphorylation of GSK-3β (Ser9) by approximately 35% ($F_{1,28} = 10.43$, $P < 0.01$) in the wild type and totally rescued phosphorylation of GSK-3β (Ser9) in the hippocampus of the fragile X mice ($F_{1,28} = 11.96$, $P < 0.01$).

Bryostatin-1 Prevents the Loss of Mature Dendritic Spines and Pre- and Postsynaptic Membranes and Presynaptic Vesicles in the Fragile X Mice. After water maze learning, dendritic spines on individual apical dendritic shafts of the CA1 pyramidal neurons (stratum radiatum) were stained with DiI and imaged with confocal microscopy by serial scanning, three-dimensional reconstruction, and a double-blind analysis (unknown subject and treatment; Fig. 2A). There was a significant overall group difference for mushroom-shaped spine density ($F_{3,94} = 2.959$, $P < 0.05$; Fig. 2B) and all-shape dendritic spine (mushroom, thin, and stubby spines together; $F_{3,94} = 4.245$, $P < 0.01$; Fig. 2C). Both mushroom-shaped spine ($P < 0.05$) and all-shape dendritic spine ($P < 0.01$) densities were significantly lower in the fragile X mice (Fig. 2, B and C). A significant overall group difference was found for the density of immature dendritic spines ($F_{3,94} = 8.347$, $P < 0.001$; Fig. 2, A and D). We found a significant ($P < 0.001$) increase in immature dendritic spine density in the fragile X mice, versus the wild type (Fig. 2D).

Bryostatin-1 significantly reduced the density of immature dendritic spines ($P < 0.01$; Fig. 2D), but increased the density of mushroom and all dendritic spines ($P < 0.01$; Fig. 2, B and C), suggesting that bryostatin-1 enhanced the transformation of immature dendritic spines to the mature dendritic spines.

Immunohistochemistry and confocal microscopy were used to study the densities of presynaptic membranes (GAP-43

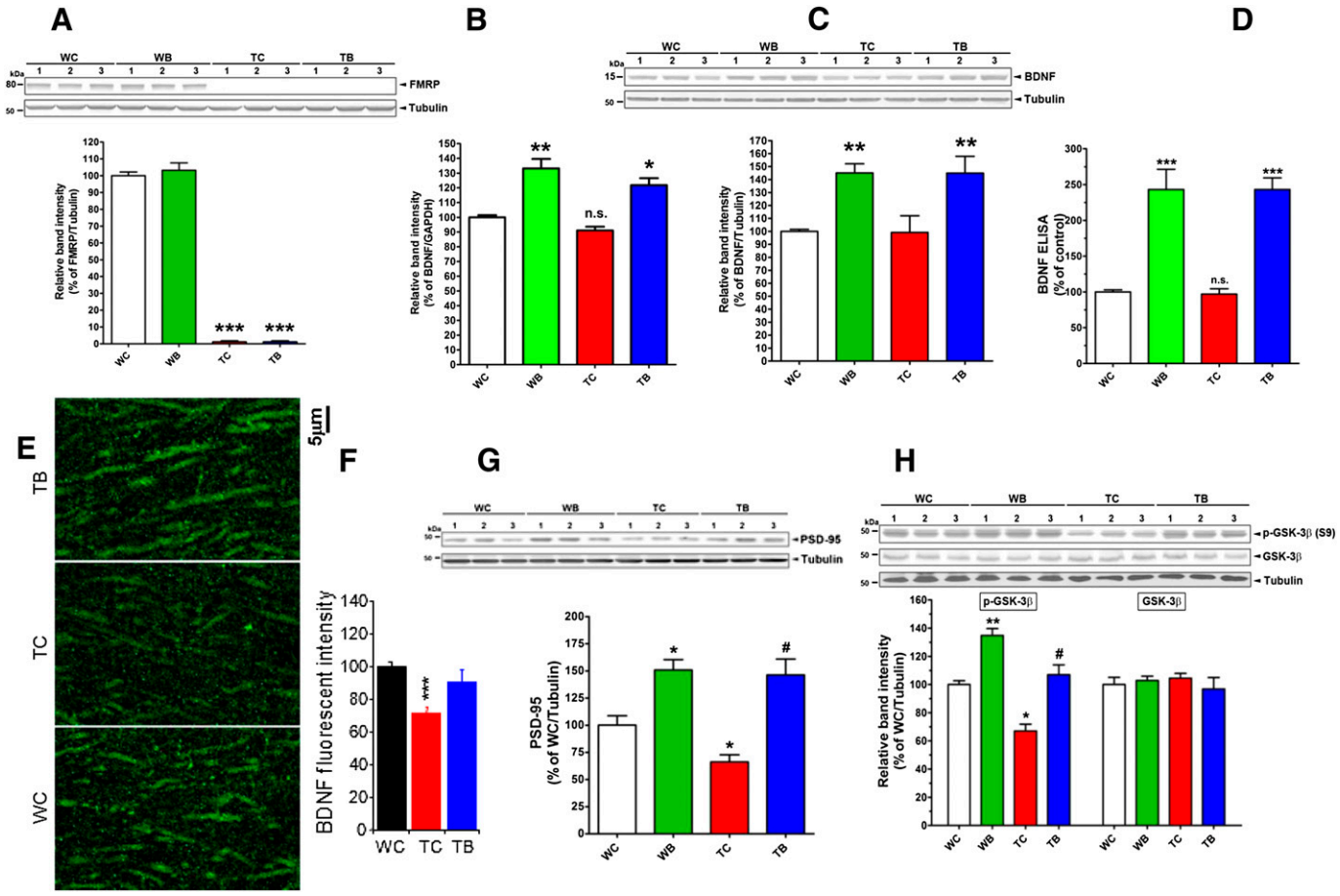

Fig. 1. Bryostatin-1 does not alter FMRP but increases BDNF expression/level, PSD-95, and inhibitory phosphorylation of GSK-3β in the hippocampus. (A) Western blot analysis using anti-FMRP antibody. Quantitative data showing each band-intensity normalized to α-tubulin staining in the WC group. (B) RT-qPCR analysis with specific primers against BDNF and GAPDH as the control. (C) Western blot analysis showing BDNF level, normalized to α-tubulin levels for the same Western blot lane. (D) BDNF ELISA assay. (E) Confocal microscopy of BDNF in hippocampal CA1 stratum radiatum, showing high level of BDNF immunofluorescence in the long profile of dendritic shafts. (F) Bryostatin-1 rescued a decrease in BDNF (N = 28–49 hippocampal CA1 areas). (G) Western blot analysis showing PSD-95 level. (H) Western blot analysis showing GSK-3β and phospho-GSK-3β (Ser9) levels. All data are presented as means ± S.E.M. from three or four animals. The same abbreviations are used in this figure and the figures that follow: WC, wild type with vehicle; WB, wild-type with bryostatin-1; TC, fragile X mice with vehicle; TB, fragile X mice with bryostatin-1; n.s., not significant. *$P < 0.05$; **$P < 0.01$; ***$P < 0.001$; #$P < 0.01$, compared with TC.

grains) and postsynaptic membranes (neurogranin grains) in the CA1 stratum radiatum (Fig. 2E). An analysis of variance revealed a significant overall group difference for presynaptic membranes ($F_{3,139} = 4.753$, $P < 0.01$; Fig. 2F) and postsynaptic membranes ($F_{3,167} = 7.713$, $P < 0.001$; Fig. 2G). Compared with the wild type, the fragile X mice had lower density of presynaptic membranes (Fig. 2F; $P < 0.01$) and postsynaptic membranes (Fig. 2G; $P < 0.001$) that were reversed by bryostatin-1 ($P < 0.05$).

The presynaptic vesicle membrane protein synaptophysin was used as a marker for presynaptic axon boutons (Graham and Redman, 1994). At the resolution of the confocal microscope, one synaptophysin granule equals one presynaptic axonal bouton/terminal (Fig. 2H). No significant group differences were found for the number of synaptophysin-labeled endings (Fig. 2I), suggesting that the number of the axon boutons was not affected by the loss of FMRP or bryostatin-1.

The concentration of presynaptic vesicles was studied by measuring fluorescence intensity of the presynaptic vesicle membrane synaptophysin. There was a significant overall group difference for synaptophysin intensity ($F_{3,122} = 3.431$, $P < 0.01$; Fig. 2J). The concentration of presynaptic vesicles decreased in the fragile X mice, versus the wild type ($P < 0.01$). In the fragile X mice treated with bryostatin-1, the presynaptic vesicle density was restored ($P < 0.01$) and reached a level higher ($P < 0.01$) than that in the wild type.

Density of synapses in the hippocampal CA1 stratum radiatum was also studied with electron microscopy (a double-blind analysis). There were significant overall group differences for synaptic density ($F_{2,114} = 2.968$, $P < 0.05$; Fig. 3, A and B) and presynaptic vesicle concentration within axonal boutons ($F_{2,114} = 8.121$, $P < 0.001$; Fig. 3, C and D). The fragile X mice had lower synaptic density (Fig. 3, A and B; $P < 0.05$) and presynaptic vesicle concentration (Fig. 3, C and D; $P < 0.01$), versus the wild type. Bryostatin-1 reversed the decrease in synaptic density in the fragile X mice (Fig. 3, A and B; $P < 0.05$). With bryostatin-1, the reduction of presynaptic vesicle number was not only rescued ($P < 0.001$; the fragile X mice + bryostatin-1 versus the fragile X mice) but also enhanced ($P < 0.05$; the fragile X mice + bryostatin-1 versus the wild type; Fig. 3, C and D), confirming the results in Fig. 2J.

As one dendritic spine may form more than one synapse, we further assessed the density of all dendritic spines, using an antibody against the dendritic spine–specific protein

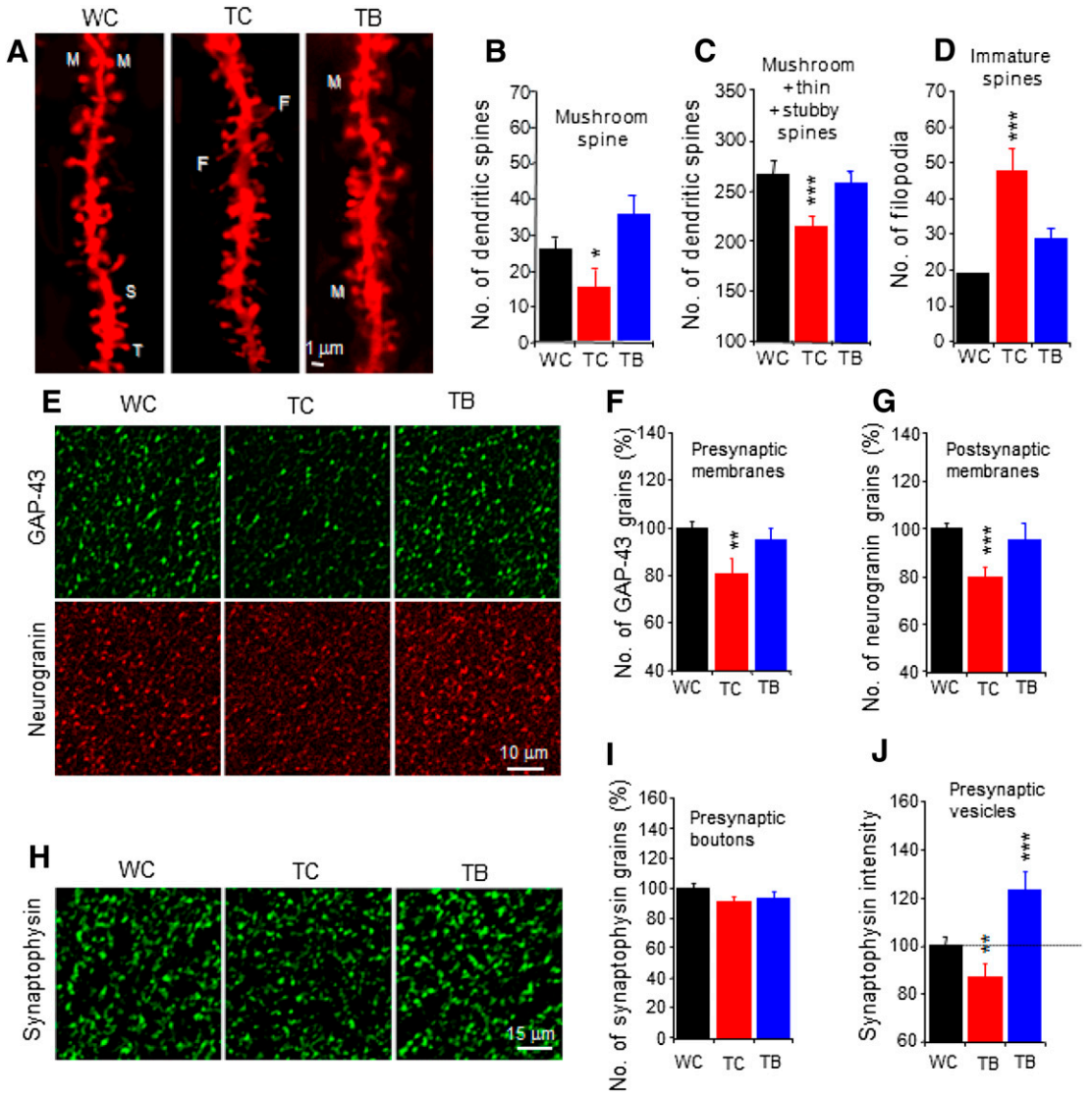

Fig. 2. Bryostatin-1 prevents the loss of mature dendritic spines and an increase in immature spines and protects the losses of pre- and postsynaptic membranes and presynaptic vesicles in the fragile X mice. (A) Confocal microscopy of dendritic spines stained with DiI. (B) Quantitative analysis of the numbers of mushroom-shape dendritic spines. (C) All mature dendritic spines (mushroom, thin, and stubby spines together). (D) Immature dendritic spines per 100-μm dendritic shaft. (E) Confocal microscopy of the immunohistochemistry of the presynaptic membrane marker GAP-43 and the postsynaptic membrane marker neurogranin. Bryostatin-1 prevented decreases in pre- (F) and postsynaptic membranes (G). (H) Confocal microscopy and immunohistochemistry of the presynaptic vesicle membrane protein synaptophysin. (I) The number of presynaptic axonal boutons (synaptophysin grains). (J) Effects of bryostatin-1 on the presynaptic vesicle concentration (synaptophysin fluorescence intensity) in axonal boutons. Data are shown as means ± S.E.M, n = 21–34 dendritic shafts or 28–61 hippocampal CA1 areas per experimental conditions from three to six animals. For simplicity, illustration of WB is not shown. $^{*}P < 0.05$; $^{**}P < 0.01$; $^{***}P < 0.001$.

spinophilin (Fig. 3E), A significant group difference was found ($F_{3,149} = 15.273$, $P < 0.001$). Bryostatin-1 increased dendritic spine density in the fragile X mice ($P < 0.001$; Fig. 3F), suggesting that the bryostatin-1–induced increase in synaptic density is correlated with an increase in the number of dendritic spines rather than an increase in multiple synapses of preexisting dendritic spines.

Bryostatin-1 Restored Spatial Learning and Memory of the Fragile X Mice but Did Not Alter Sensorimotor Ability. There were significant group differences in learning ($F_{3,623} = 5.214$, $P = 0.001$; Fig. 4A). Bryostatin-1 significantly improved the learning of the fragile X mice (the fragile X mice versus the fragile X mice with bryostatin-1: $F_{1,319} = 15.556$, $P < 0.001$) to the level of the controls (the wild-type versus the fragile X mice with bryostatin-1: $F_{1,319} = 0.827$, $P > 0.05$), indicating that bryostatin-1 repaired the learning of the fragile X mice.

The results in the probe test (Fig. 4, B–E) were analyzed using the target quadrant ratio (dividing the target quadrant distance by the average of the nontarget quadrant values during the probe test; Fig. 4F). There were significant group differences in the ratio ($F_{3,38} = 3.016$, $P < 0.05$), indicating differences in the spatial memory. Detailed analysis reveals that bryostatin-1 significantly improved the memory recall in the fragile X mice versus the mice without bryostatin-1 ($F_{1,19} = 6.640$, $P < 0.05$), to the level of the control (the wild-type versus the fragile X mice + bryostatin-1: $F_{1,15} = 0.028$, $P > 0.05$).

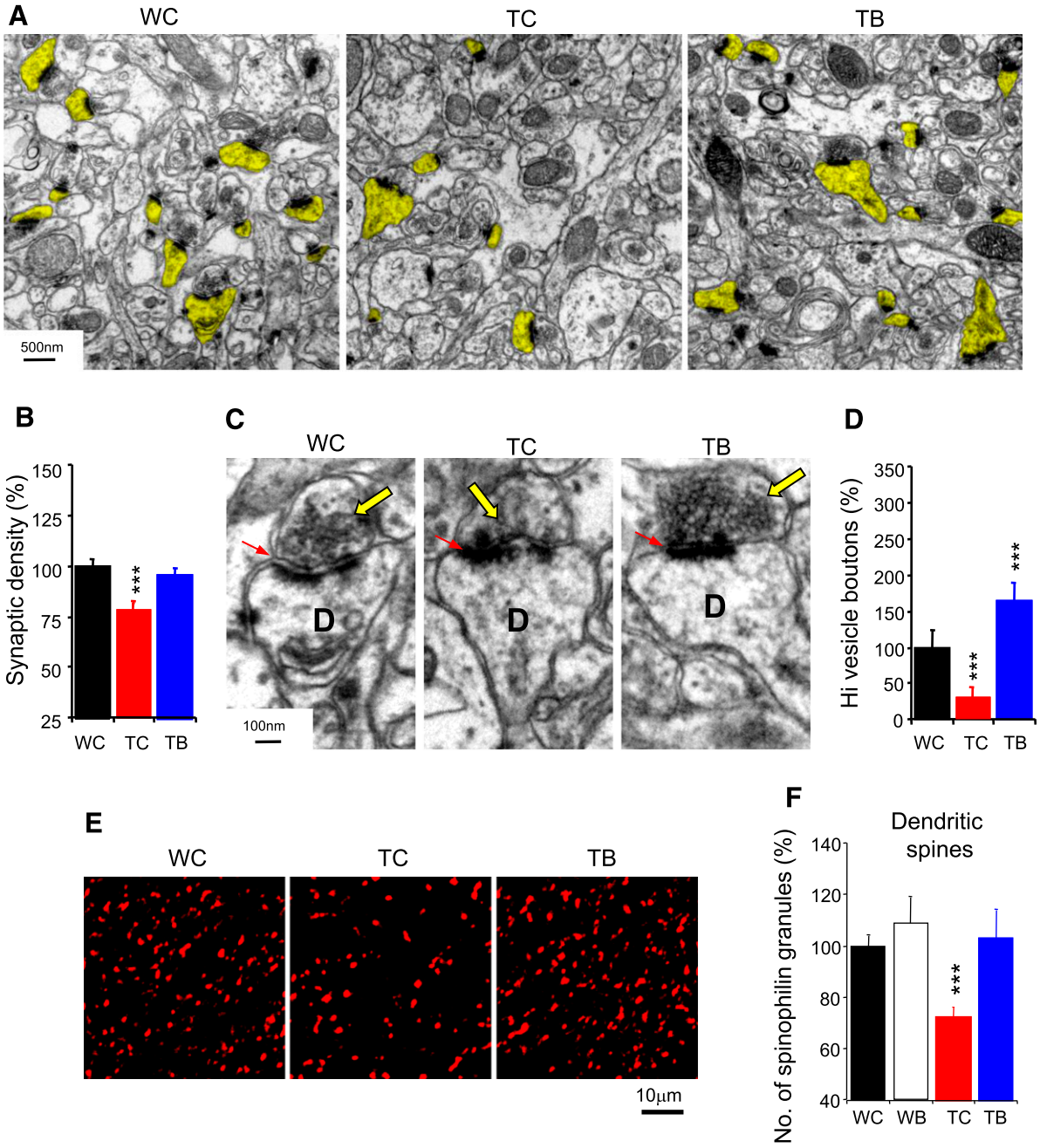

Fig. 3. Bryostatin-1 restores the number of synapses in fragile X mice. (A) Electron microscopy (EM) of the stratum radiatum in the right dorsal hippocampal CA1 area. Dendritic spines are highlighted in yellow. (B) EMs at higher magnification show dendritic spines forming synapses (red arrows) with presynaptic axonal boutons that contain presynaptic vesicles (yellow arrows). Bryostatin prevented the loss of synaptic density (A) and (B) and presynaptic vesicle concentration (C) and (D) within 8 × 8 × 0.07 μm of the CA1 stratum radiatum. (E) Confocal microscopy of dendritic spines immunostained with the dendritic spine-specific protein spinophilin in hippocampal CA1 stratum radiatum revealed that bryostatin (F) increased the maturation of dendritic spine. Data are shown as means ± S.E.M, n = 38–61 hippocampal CA1 areas per experimental conditions from three animals. For simplicity, illustration of WB is not shown. ***$P < 0.001$.

A visible platform test, determined after the probe test, revealed no significant group differences ($F_{3,38} = 1.042$; $P > 0.05$) (Fig. 4G), indicating that there were no group differences in sensorimotor ability or escape motivation.

Discussion

The results of the present study reveal a novel pharmacologic profile of bryostatin-1 (Nelson et al., 2008; DeChristopher et al., 2012) for treating FXS after the FXS phenotypes have already been established in the fragile X mice (Bhattacharya and Klann, 2012). Bryostatin-1 rescues the hippocampus from the FXS phenotypes, including a decrease in PSD-95, a decrease in GSK-3β phosphorylation, a decrease in density of presynaptic and postsynaptic membranes, an increase in immature synapses, a decrease in learning-induced mature synapses, and an impairment of hippocampus-dependent spatial learning and memory. Learned-induced formation of dendritic spines

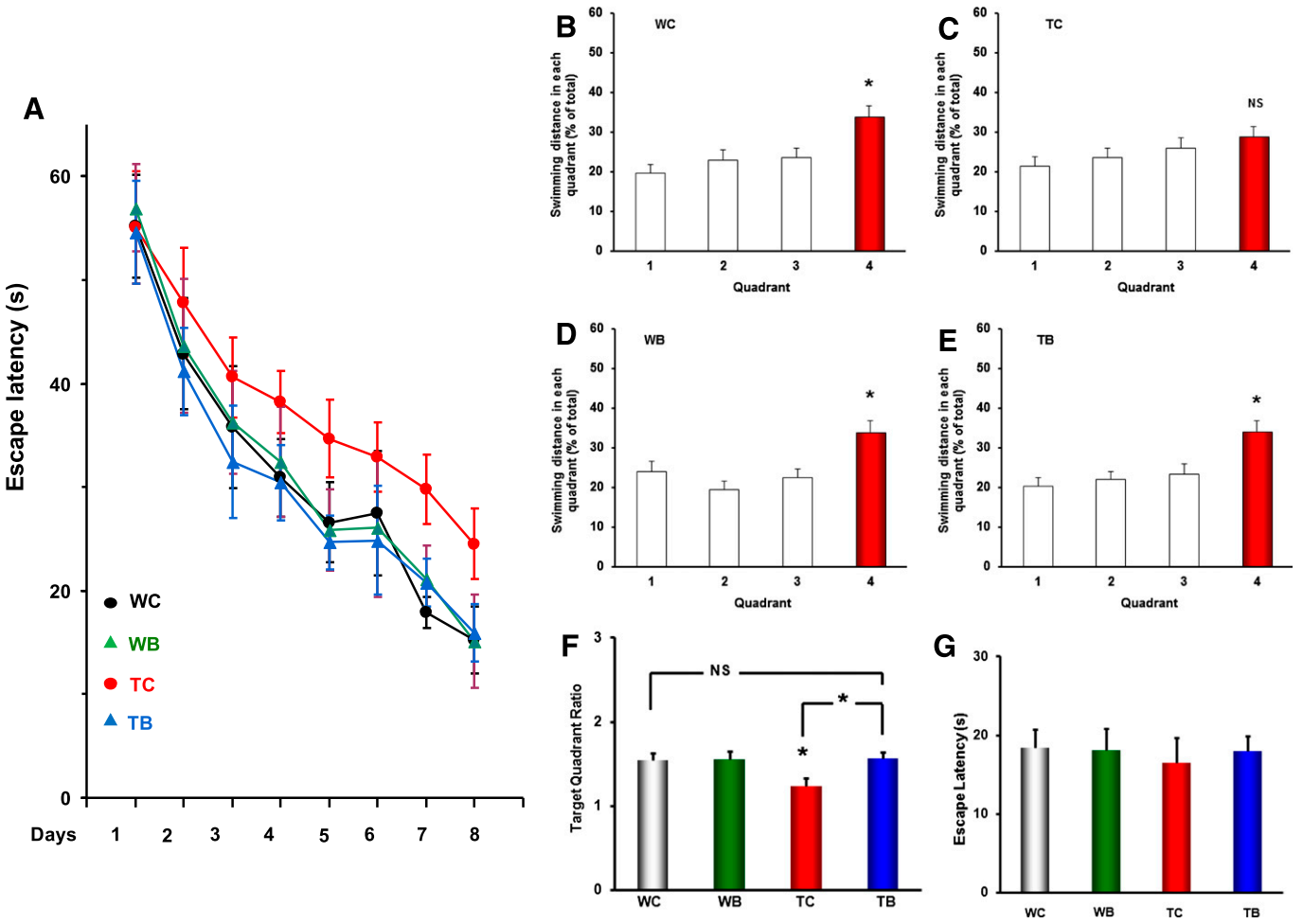

Fig. 4. Bryostatin-1 restores spatial learning and memory in fragile X mice. (A) Water maze learning. Data are shown as means ± S.E.M., using the daily two trials as a block. (B–F) Results of the probe tests after the training trials shown as the distance in each quadrant (B–F). Quadrant 4 was the target quadrant. (F) Target quadrant ratio. (G) Escape latency during the visible platform test. *$P < 0.05$; NS: $P > 0.05$.

is severely impaired in the fragile X mice (Padmashri et al., 2013), probably involving a loss of some dendritic channels (Routh et al., 2013), but can be rescued with bryostatin-1 treatment.

FMRP is an mRNA-binding translation regulator that mediates activity-dependent control of synaptic structure and function (Niere et al., 2012). Its lack results in an overactivity of the mGluRs, a decreased GABAergic system or delayed developmental switch in GABA polarity (D'Hulst et al., 2006; Olmos-Serrano et al., 2010; He et al., 2014), and an elevated activity of GSK-3β (Guo et al., 2012). Potential therapeutics, therefore, include mGluR inhibitors (Vinueza Veloz et al., 2012), GABAergic enhancers (D'Hulst and Kooy, 2007; Olmos-Serrano et al., 2010; Paluszkiewicz et al., 2011; Heulens et al., 2012), and inhibitors of GSK-3β (Yuskaitis et al., 2010; Guo et al., 2012). Because intellectual ability, as well as retardation (Wang et al., 2012) involves multiple players in signal processing, bryostatin-1–like agents, for their multitargeting actions, may represent a more effective class of therapeutics than agents that target a single factor in this complex pathologic process (Vislay et al., 2013).

First, some PKC isozymes play an essential role in various phases and types of learning and memory (Alkon et al., 2005). PKC activators not only increase activity of PKC isozymes and thereby restore PKC signal activity, including neurotrophic activity (Alkon et al., 2007; Sun et al., 2008), synaptic/structural remodeling, and synaptogenesis, but also reduce the accumulation of neurotoxic amyloid (Alkon et al., 2007; Hongpaisan et al., 2011), which may play pathologic roles in the fragile X mice (Westmark et al., 2011). The effects of bryostatin-1 on disorder-induced learning and memory impairments are evidenced in the present study in that it fully rescued the spatial learning and memory in the fragile X mice. The results are consistent with an earlier observation that infusion of BDNF restored synaptic function in slices from the fragile X mice (Lauterborn et al., 2007). PKCα,ε enhances BDNF expression and via the mRNA-stabilizing protein HuD increases expression of other synaptogenic factors, such as GAP-43, insulin-like growth factor, neurotrophic factor, and nerve growth factor (Nelson et al., 2008).

Second, PKCε and other isoforms are known to phosphorylate mGluR5 at multiple sites, inducing a relatively rapid form of desensitization (Gereau and Heinemann, 1998), an action that directly targets the mGluR-mediated overactivity.

Third, bryostatin-1 effectively increases the hippocampal PSD-95 levels in the fragile X mice. The mGluR5 dysfunction includes an altered Homer scaffold interaction (Ronesi et al., 2012). Consistent with others' findings, the synaptic scaffold

protein PSD-95 was downregulated in the hippocampus, probably because of an alteration in mRNA stability (Zalfa et al., 2007).

Fourth, bryostatin-1 rescues the GSK-3β level to that of the wild type. GSK-3β is a core component of FXS pathology (Yuskaitis et al., 2010) and is mainly regulated by phosphorylation on an N-terminal serine, Ser-9-GSK-3β, for its inhibition. This inhibitory serine-phosphorylation of GSK-3 is impaired in the fragile X mice (Min et al., 2009) but can be rescued by bryostatin-1.

Fifth, bryostatin-1 induces transformation of immature dendritic spines to mature synapses in the hippocampus of the fragile X mice and thus avoids the undesired impact of a pure mGluR inhibition on spine immaturity (Cruz-Martin et al., 2010). Bryostain-1 was administered at a dose at which it promotes learning-induced synaptogenesis and synaptic maturation (Hongpaisan and Alkon 2007, Hongpaisan et al., 2011). Mice lacking expression of *FMR1* show an abundance of dense, immature dendritic spines (Scotto-Lomassese et al., 2011), as in FXS patients (Grossman et al., 2006). The hyperabundance of immature-looking lengthened dendritic spines could be the results of a failed/delayed maturation (Cruz-Martin et al., 2010; Harlow et al., 2010) and activity-dependent synaptic elimination (Pfeiffer et al., 2010). In short, bryostatin-1–like agents (Sun and Alkon, 2005; Nelson et al., 2009; DeChristopher et al., 2012) may have important therapeutic value for the treatment of adult FXS.

Authorship Contributions

Participated in research design: Sun, Hongpaisan, Lim, Alkon.

Conducted experiments: Sun, Hongpaisan, Lim.

Performed data analysis: Sun, Hongpaisan, Lim.

Wrote or contributed to the writing of the manuscript: Sun, Hongpaisan, Lim, Alkon.

References

Alkon DL, Epstein H, Kuzirian A, Bennett MC, and Nelson TJ (2005) Protein synthesis required for long-term memory is induced by PKC activation on days before associative learning. *Proc Natl Acad Sci USA* **102**:16432–16437.

Alkon DL, Sun M-K, and Nelson TJ (2007) PKC signaling deficits: a mechanistic hypothesis for the origins of Alzheimer's disease. *Trends Pharmacol Sci* **28**:51–60.

Ashley CT, Jr, Wilkinson KD, Reines D, and Warren ST (1993) FMR1 protein: conserved RNP family domains and selective RNA binding. *Science* **262**:563–566.

Bhattacharya A and Klann E (2012) Fragile X syndrome therapeutics S(C)TEP through the developmental window. *Neuron* **74**:1–3.

Bhogal B and Jongens TA (2010) Fragile X syndrome and model organisms: identifying potential routes of therapeutic intervention. *Dis Model Mech* **3**:693–700.

Connor SA, Hoeffer CA, Klann E, and Nguyen PV (2011) Fragile X mental retardation protein regulates heterosynaptic plasticity in the hippocampus. *Learn Mem* **18**:207–220.

Cruz-Martín A, Crespo M, and Portera-Cailliau C (2010) Delayed stabilization of dendritic spines in fragile X mice. *J Neurosci* **30**:7793–7803.

Darnell JC and Klann E (2013) The translation of translational control by FMRP: therapeutic targets for FXS. *Nat Neurosci* **16**:1530–1536.

DeChristopher BA, Loy BA, Marsden MD, Schrier AJ, Zack JA, and Wender PA (2012) Designed, synthetically accessible bryostatin analogues potently induce activation of latent HIV reservoirs in vitro. *Nat Chem* **4**:705–710.

D'Hulst C and Kooy RF (2007) The $GABA_A$ receptor: a novel target for treatment of fragile X? *Trends Neurosci* **30**:425–431.

D'Hulst C, De Geest N, Reeve SP, Van Dam D, De Deyn PP, Hassan BA, and Kooy RF (2006) Decreased expression of the $GABA_A$ receptor in fragile X syndrome. *Brain Res* **1121**:238–245.

Garber KB, Visootsak J, and Warren ST (2008) Fragile X syndrome. *Eur J Hum Genet* **16**:666–672.

Gereau RW 4th and Heinemann SF (1998) Role of protein kinase C phosphorylation in rapid desensitization of metabotropic glutamate receptor 5. *Neuron* **20**:143–151.

Gonçalves JT, Anstey JE, Golshani P, and Portera-Cailliau C (2013) Circuit level defects in the developing neocortex of fragile X mice. *Nat Neurosci* **16**:903–909.

Graham B and Redman S (1994) A simulation of action potentials in synaptic boutons during presynaptic inhibition. *J Neurophysiol* **71**:538–549.

Grossman AW, Aldridge GM, Weiler IJ, and Greenough WT (2006) Local protein synthesis and spine morphogenesis: fragile X syndrome and beyond. *J Neurosci* **26**: 7151–7155.

Guo W, Murthy AC, Zhang L, Johnson EB, Schaller EG, Allan AM, and Zhao X (2012) Inhibition of GSK3β improves hippocampus-dependent learning and rescues neurogenesis in a mouse model of fragile X syndrome. *Hum Mol Genet* **21**:681–691.

Hajós M (2014) Portraying inhibition of metabotropic glutamate receptor 5 in fragile X mice. *Biol Psychiatry* **75**:177–178.

Harlow EG, Till SM, Russell TA, Wijetunge LS, Kind P, and Contractor A (2010) Critical period plasticity is disrupted in the barrel cortex of FMR1 knockout mice. *Neuron* **65**:385–398.

He Q, Nomura T, Xu J, and Contractor A (2014) The developmental switch in GABA polarity is delayed in Fragile X mice. *J Neurosci* **34**:446–450.

Heulens I, D'Hulst C, Van Dam D, De Deyn PP, and Kooy RF (2012) Pharmacological treatment of Fragile X syndrome with GABAergic drugs in a knockout mouse model. *Behav Brain Res* **229**:244–249.

Hongpaisan J and Alkon DL (2007) A structural basis for enhancement of long-term associative memory in single dendritic spines regulated by PKC. *Proc Natl Acad Sci USA* **104**:19571–19576.

Hongpaisan J, Sun M-K, and Alkon DL (2011) PKC ε activation prevents synaptic loss, Aβ elevation, and cognitive deficits in Alzheimer's disease transgenic mice. *J Neurosci* **31**:630–643.

Kaufmann WE, Abrams MT, Chen W, and Reiss AL (1999) Genotype, molecular phenotype, and cognitive phenotype: correlations in Fragile X syndrome. *Am J Med Genet* **83**:286–295.

Kirov SA, Petrak LJ, Fiala JC, and Harris KM (2004) Dendritic spines disappear with chilling but proliferate excessively upon rewarming of mature hippocampus. *Neuroscience* **127**:69–80.

Koekkoek SK, Yamaguchi K, Milojkovic BA, Dortland BR, Ruigrok TJ, Maex R, De Graaf W, Smit AE, VanderWerf F, and Bakker CE, et al. (2005) Deletion of FMR1 in Purkinje cells enhances parallel fiber LTD, enlarges spines, and attenuates cerebellar eyelid conditioning in fragile X syndrome. *Neuron* **47**: 339–352.

Lauterborn JC, Rex CS, Kramár E, Chen LY, Pandyarajan V, Lynch G, and Gall CM (2007) Brain-derived neurotrophic factor rescues synaptic plasticity in a mouse model of Fragile X syndrome. *J Neurosci* **27**:10685–10694.

Ludwig AL, Espinal GM, Pretto DI, Jamal AL, Arque G, Tassone F, Berman RF, and Hagerman PJ (2014) CNS expression of murine Fragile X protein (FMRP) as a function of CGG-repeat size. *Hum Mol Genet* [published ahead of print].

Lüscher C and Huber KM (2010) Group 1 mGluR-dependent synaptic long-term depression: mechanisms and implications for circuitry and disease. *Neuron* **65**: 445–459.

McLennan Y, Polussa J, Tassone F, and Hagerman R (2011) Fragile X syndrome. *Curr Genomics* **12**:216–224.

Min WW, Yuskaitis CJ, Yan Q, Sikorski C, Chen S, Jope RS, and Bauchwitz RP (2009) Elevated glycogen synthase kinase-3 activity in fragile X mice: key metabolic regulator with evidence for treatment potential. *Neuropharmacology* **56**: 463–472.

Nelson TJ, Sun M-K, Hongpaisan J, and Alkon DL (2008) Insulin, PKC signaling pathways and synaptic remodeling during memory storage and neuronal repair. *Eur J Pharmacol* **585**:76–87.

Nelson TJ, Cui C, Luo Y, and Alkon DL (2009) Reduction of beta-amyloid levels by novel protein kinase C (epsilon) activators. *J Biol Chem* **284**:34514–34521.

Niere F, Wilkerson JR, and Huber KM (2012) Evidence for a Fragile X mental retardation protein-mediated translational switch in metabotropic glutamate receptor-triggered Arc translation and long-term depression. *J Neurosci* **32**: 5924–5936.

Olmos-Serrano JL, Paluszkiewicz SM, Martin BS, Kaufmann WE, Corbin JG, and Huntsman MM (2010) Defective GABAergic neurotransmission and pharmacological rescue of neuronal hyperexcitability in the amygdala in a mouse model of Fragile X syndrome. *J Neurosci* **30**:9929–9938.

Padmashri R, Reiner BC, Suresh A, Spartz E, and Dunaevsky A (2013) Altered structural and functional synaptic plasticity with motor skill learning in a mouse model of Fragile X syndrome. *J Neurosci* **33**:19715–19723.

Paluszkiewicz SM, Martin BS, and Huntsman MM (2011) Fragile X syndrome: the GABAergic system and circuit dysfunction. *Dev Neurosci* **33**:349–364.

Pfeiffer BE, Zang T, Wilkerson JR, Taniguchi M, Maksimova MA, Smith LN, Cowan CW, and Huber KM (2010) Fragile X mental retardation protein is required for synapse elimination by the activity-dependent transcription factor MEF2. *Neuron* **66**:191–197.

Ronesi JA, Collins KA, Hays SA, Tsai NP, Guo W, Birnbaum SG, Hu JH, Worley PF, Gibson JR, and Huber KM (2012) Disrupted Homer scaffolds mediate abnormal mGluR5 function in a mouse model of Fragile X syndrome. *Nat Neurosci* **15**: 431–440, S1.

Routh BN, Johnston D, and Brager DH (2013) Loss of functional A-type potassium channels in the dendrites of CA1 pyramidal neurons from a mouse model of Fragile X syndrome. *J Neurosci* **33**:19442–19450.

Sabaratnam M, Murthy NV, Wijeratne A, Buckingham A, and Payne S (2003) Autistic-like behaviour profile and psychiatric morbidity in fragile X syndrome: a prospective ten-year follow-up study. *Eur Child Adolesc Psychiatry* **12**:172–177.

Santoro MR, Bray SM, and Warren ST (2012) Molecular mechanisms of Fragile X syndrome: a twenty-year perspective. *Annu Rev Pathol* **7**:219–245.

Schaeffer C, Beaulande M, Ehresmann C, Ehresmann B, and Moine H (2003) The RNA binding protein FMRP: new connections and missing links. *Biol Cell* **95**: 221–228.

Scotto-Lomassese S, Nissant A, Mota T, Néant-Féry M, Oostra BA, Greer CA, Lledo PM, Trembleau A, and Caillé I (2011) Fragile X mental retardation protein regulates new neuron differentiation in the adult olfactory bulb. *J Neurosci* **31**: 2205–2215.

Sorra KE and Harris KM (2000) Overview on the structure, composition, function, development, and plasticity of hippocampal dendritic spines. *Hippocampus* **10**: 501–511.

Sun M-K and Alkon DL (2005) Dual effects of bryostatin-1 on spatial memory and depression. *Eur J Pharmacol* **512**:43–51.
Sun M-K, Hongpaisan J, Nelson TJ, and Alkon DL (2008) Poststroke neuronal rescue and synaptogenesis mediated in vivo by protein kinase C in adult brains. *Proc Natl Acad Sci USA* **105**:13620–13625.
Szallasi Z, Smith CB, Pettit GR, and Blumberg PM (1994) Differential regulation of protein kinase C isozymes by bryostatin 1 and phorbol 12-myristate 13-acetate in NIH 3T3 fibroblasts. *J Biol Chem* **269**:2118–2124.
Van der Molen MJ, Huizinga M, Huizenga HM, Ridderinkhof KR, Van der Molen MW, Hamel BJ, Curfs LM, and Ramakers GJ (2010) Profiling fragile X syndrome in males: strengths and weaknesses in cognitive abilities. *Res Dev Disabil* **31**:426–439.
Vinueza Veloz MF, Buijsen RA, Willemsen R, Cupido A, Bosman LW, Koekkoek SK, Potters JW, Oostra BA, and De Zeeuw CI (2012) The effect of an mGluR5 inhibitor on procedural memory and avoidance discrimination impairments in Fmr1 KO mice. *Genes Brain Behav* **11**:325–331.
Verkerk AJ, Pieretti M, Sutcliffe JS, Fu YH, Kuhl DP, Pizzuti A, Reiner O, Richards S, Victoria MF, and Zhang FP, et al. (1991) Identification of a gene (FMR-1) containing a CGG repeat coincident with a breakpoint cluster region exhibiting length variation in Fragile X syndrome. *Cell* **65**:905–914.
Vislay RL, Martin BS, Olmos-Serrano JL, Kratovac S, Nelson DL, Corbin JG, and Huntsman MM (2013) Homeostatic responses fail to correct defective amygdala inhibitory circuit maturation in Fragile X syndrome. *J Neurosci* **33**: 7548–7558.
Wang X, Snape M, Klann E, Stone JG, Singh A, Petersen RB, Castellani RJ, Casadesus G, Smith MA, and Zhu X (2012) Activation of the extracellular signal-regulated kinase pathway contributes to the behavioral deficit of fragile X-syndrome. *J Neurochem* **121**:672–679.
Weiler IJ, Irwin SA, Klintsova AY, Spencer CM, Brazelton AD, Miyashiro K, Comery TA, Patel B, Eberwine J, and Greenough WT (1997) Fragile X mental retardation protein is translated near synapses in response to neurotransmitter activation. *Proc Natl Acad Sci USA* **94**:5395–5400.
Wender PA, Cribbs CM, Koehler KF, Sharkey NA, Herald CL, Kamano Y, Pettit GR, and Blumberg PM (1988) Modeling of the bryostatins to the phorbol ester pharmacophore on protein kinase C. *Proc Natl Acad Sci USA* **85**:7197–7201.
Wender PA, Baryza JL, Brenner SE, DeChristopher BA, Loy BA, Schrier AJ, and Verma VA (2011) Design, synthesis, and evaluation of potent bryostatin analogs that modulate PKC translocation selectivity. *Proc Natl Acad Sci USA* **108**: 6721–6726.
Westmark CJ, Westmark PR, O'Riordan KJ, Ray BC, Hervey CM, Salamat MS, Abozeid SH, Stein KM, Stodola LA, and Tranfaglia M, et al. (2011) Reversal of Fragile X phenotypes by manipulation of AβPP/Aβ levels in Fmr1KO mice. *PLoS ONE* **6**:e26549.
Yang JC, Simon C, Niu YQ, Bogost M, Schneider A, Tassone F, Seritan A, Grigsby J, Hagerman PJ, and Hagerman RJ, et al. (2013) Phenotypes of hypofrontality in older female Fragile X premutation carriers. *Ann Neurol* **74**:275–283.
Yuskaitis CJ, Mines MA, King MK, Sweatt JD, Miller CA, and Jope RS (2010) Lithium ameliorates altered glycogen synthase kinase-3 and behavior in a mouse model of fragile X syndrome. *Biochem Pharmacol* **79**:632–646.
Zalfa F, Eleuteri B, Dickson KS, Mercaldo V, De Rubeis S, di Penta A, Tabolacci E, Chiurazzi P, Neri G, and Grant SG, et al. (2007) A new function for the fragile X mental retardation protein in regulation of PSD-95 mRNA stability. *Nat Neurosci* **10**:578–587.

Address correspondence to: Miao-Kun Sun, Blanchette Rockefeller Neuroscience Institute, 8 Medical Center Dr., Morgantown, WV 26505. E-mail: masun@brni.org